



Toothed wheel needleless electrospinning: a versatile way to fabricate uniform and finer nanomembrane

Adnan Ahmad¹ , Usman Ali^{3,4} , Ahsan Nazir¹ , Amir Shahzad¹ , Zubair Khaliq^{1,2,*} , Muhammad Bilal Qadir^{1,2,*} , Muhammad Amir Khan¹ , Sultan Ali¹ , M. Aamir Hassan⁴ , Sharjeel Abid¹ , Rizwan Tahir¹ , and Bushra Mushtaq¹

¹ Faculty of Engineering and Technology, National Textile University, Faisalabad 37610, Pakistan

² Department of Organic and Nano Engineering, Hanyang University, Seoul 04763, South Korea

³ Institute for Frontier Materials, Deakin University, Geelong, VIC 3216, Australia

⁴ TTRC, College of Textile Engineering, Bahauddin Zakariya University, Multan 60800, Pakistan

Received: 14 June 2019

Accepted: 23 July 2019

Published online:

31 July 2019

© Springer Science+Business Media, LLC, part of Springer Nature 2019

ABSTRACT

Needleless electrospinning is an effective approach to fabricate the nanofibers at high throughput. However, the uniform distribution of nanofibers with finer diameter still needs improvement. In this study, optimization of needleless electrospun polyacrylonitrile (PAN) nanofibers was carried out using an effectively designed toothed wheel spinneret, which improved the nanofiber uniform distribution with finer diameter. Finite element method showed that the electric field norms were highly concentrated at toothed wheel edges. Optimized beadless PAN nanofibers with narrow diameter distribution were obtained at 6 w/v% polymer concentration, 50 kV applied voltage, and 23 cm collecting distance. Highest tensile strength of 100 cN at 7 w/v% concentration showed that the resultant membrane had good mechanical properties. The air permeability of 15 mm/s was obtained at 6 w/v% indicating good insulating behavior of the PAN nanofiber membrane. This study proved that the toothed wheel spinneret has the potential to improve the electrospinning process for the development of uniform nanofibrous membrane at a high production rate.

Introduction

Nanomaterials are the unique and versatile materials which possess exceptional characteristics and find a wide range of application in the field of medical, technical textile, energy storage devices, etc. [1–14]. Electrospinning is a simple and distinguished technique used for the synthesis of polymer fiber with the

diameter in the range of few micrometers to nanometers [15]. Nanofiber production rate and diameter distribution are highly affected by the solution, and process parameters such as concentration applied potential difference and collecting distance [16–19]. Electrospun nanofibers have attracted considerable attention due to its high specific surface area, excellent dimension stability, high porous

Address correspondence to E-mail: zubntu@yahoo.com; bilal_ntu81@hotmail.com

structure, and good mechanical strength [20, 21]. These exceptional attributes lead the electrospun nanofiber to very effective in the biomedical, energy storage, sensors, filtration, actuators, cosmetics, and protective textile [22–29].

Needle electrospinning has great potential to form nanofiber with unique characteristics, but it has a limitation of low productivity, which is less than 0.3 g/h. A simple and effective way to enhance the production rate is to use a large number of needles instead of a single one. This system is known as “Multi-needle electrospinning” [30]. However, this method is not very effective as the multi-needles create strong repulsive forces [31] among the adjacent jets, so it requires large working space to overcome this effect. The clogging of the polymer solution in the needles needs a cleaning system to remove the solution and for the smooth electrospinning process. Horizontal [32] and verticals tube electrospinning [33] with pores was reported as an alternative solution for multi-needle electrospinning. The pores provided the sites for the fiber generation. The technique was easily operated and needed less space compared to the older. However, high productivity and effective control of jet interference were still an issue.

In recent times, needleless electrospinning has gained great attention due to its higher productivity with eliminating the issue of large space and electric interference disturbance [34]. Magnetic assistance needleless electrospinning was introduced by Yarin and Zussman [35] to form the nanofiber. Liu and He [36] reported the bubble electrospinning to form the nanofibers. Thoppey et al. [37] fabricated the nanofiber by using the plate edge as a jet formation site. Jirsak et al. [38] reported the needleless electrospinning of nanofiber by using a metal roller spinneret.

Other spinnerets such as dual wire, bowl edge, conical wire coil, sprocket wheel, metal disk, wire electrode, roller, slot, needle disk, stepped pyramids, and hallow cone were also used to enhance the productivity of electrospinning process [39–43]. The productivity of these spinnerets was much higher compared to needle electrospinning. However, these spinnerets still have limitations such as the wider distribution of nanofiber diameter, uneven mass distribution of nanoweb, non-uniform distribution of electric field intensity, lower production rate as required for commercial scale, and required high voltage to initiate the electrospinning process.

The above-discussed issues are resolved through a new approach of needleless electrospinning containing a toothed wheel as a spinneret. The electric field distribution on the surface of the spinneret was optimized with the help of simulation software, which plays a key role in the production of electrostatic force. Moreover, fiber morphology and productivity were also studied at different polymer concentration and process parameters. These parameters were statistically evaluated to measure the significance of the individual parameter. The developed PAN nanofiber membranes were mechanically tested for practical application. Also, the air flow resistance of these membranes was investigated at different levels. This study specifies that the toothed wheel spinneret has the potential to improve the electrospinning process for the development of uniform nanofibrous membrane at a high production rate and could be used in valuable applications in the field of medical, energy devices, etc.

Experimental procedure

Materials

Polyacrylonitrile (PAN) ($M_w = 150,000$ g/mol, density = 1.184 g/cc) and *N,N*-dimethylformamide (DMF) were purchased from Sigma-Aldrich. Multiple PAN-DMF homogenous solutions ranging from 4 to 12 w/v% of concentration were prepared by magnetic stirring the mixture for 24 h at 50 °C continuously.

Synthesis of nanofiber

Fabrication of PAN nanofiber was carried out using a needleless electrospinning setup. It comprises of rotating spinneret, a rotating metal cylinder as a grounded collector, a Teflon solution bath and 100 kV Gamma high-voltage DC power supply. A toothed wheel was used as a spinneret, and the dimensions of spinneret are as thickness = 5 mm, exterior diameter = 60 mm, number of teeth = 14, pitch = 13.45 mm, and teeth size = 3 mm. The applied voltage and collecting distance were varied from 40 to 60 kV and from 19 to 24 cm, respectively. The spinneret and collecting cylinder were driven through a 12 V DC motor with opposite rotation to each other.

A series of experiments were conducted to investigate the effect of electrospinning parameters on the physical and mechanical characteristics of PAN nanofibers. The electrospinning time was kept 90 min to prepare each sample for accurate comparison of parameters.

Characterization

PAN nanofibers morphology was examined through a scanning electron microscope (SEM) from Quanta 250 FEI at different magnification levels at 5–15 kV. A thin layer of gold was developed on the sample through sputter coating. The SEM images were taken from different positions of nanoweb. Image J software was used to measure the PAN nanofiber diameter based on SEM images. Total of 100 readings were taken and calculated the average diameter for each sample.

Initially, the samples were kept at 200 °C for 30 min for evaporation of the solvent. The tensile strength of the electrospun mat was calculated with single fiber strength tester (Tensiometric 2.5). Each sample was cut to dimensions of 5 mm width and 10 mm length. The tensile strength tests were performed at 10 mm/min speed and 10 mm gauge length by using a 50 N load cell at a constant rate of 0.1 mm/s. The air permeability of PAN nanofiber was evaluated through Air permeability Tester MO21A. The test was performed according to testing standard ASTM D737. Total 5 readings of each sample were taken, and the average value was recorded.

Results and discussion

Electrospinning process and electric field profile

Figure 1 shows the schematic diagram of the needleless electrospinning process. In this needleless electrospinning process, the PAN polymer solution was kept in a Teflon bath. The toothed wheel spinneret was dipped into the polymer solution and continuously rotated by using a 12 DC voltage supply. The teeth of the wheel carried the polymer solution at the spinning site during its continuous rotation. The strong electric electrostatic forces were applied to the polymer solution due to the applied high voltage. When these forces overcame the surface

tension of the PAN solution, the polymer jets were raised from the boundaries of the teeth and accelerated toward the collector.

Finite element method was used for the optimization of needleless electrospinning process using toothed wheel spinneret. Electric field analysis was done through the COMSOL Multiphysics 5.0 commercial software. The geometry of the toothed wheel was sketched in COMSOL solid work frame with the dimensions of diameter = 60 mm, the number of teeth = 14, the thickness of wheel = 5 mm, and distance between adjacent teeth = 10 mm. The electric field intensity was calculated at different collecting distances and the applied voltages. The electric field can be defined as the negative gradient of potential difference as given in the equation

$$E = -\nabla V$$

here, E is the electric field, and V is the potential difference.

The geometry of the spinneret plays a vital role in the generation of a high electric field during the electrospinning process. The geometry with sharp edges is more effective for the electrospinning process as the sharp edges generate strong electric field intensity at a constant applied potential. This is because of the reason that electric field intensity is more concentrated and sharp at the teeth of the wheel spinneret in contrast to the rest of the body. This enables the spinneret to produce polymer jets at a lower applied voltage with narrow fiber diameter distribution. Figure 2a–d shows the electric field intensity profile along the axis direction, spinning direction, and spinneret rotation, respectively.

Figure 3a–d shows the distribution of electric field intensity at various applied voltages along with the electric field norm scale. The color variance of electric field intensity on varying the voltage from 40 to 70 kV predicts the stronger electric field concentration at higher applied voltage. The increase in electric intensity enhances the attenuation of charged jet and hence results in finer nanofiber diameter. Moreover, the wider distribution of the electric field at the toothed surface initiates several charged jets and increases the production rate. Figure 3e, f shows the relation of electric field intensity along the axis direction with the applied voltage and collecting distance, respectively. The highest electric field norms are 7554 kV/m calculated at 70 kV and 13 cm collecting distance.

Figure 1 Needleless electrospinning using toothed wheel spinneret. **a** Machine setup scheme, **b** spinneret, **c** spinning process with toothed wheel spinneret, **d** nanofiber web with the SEM image.

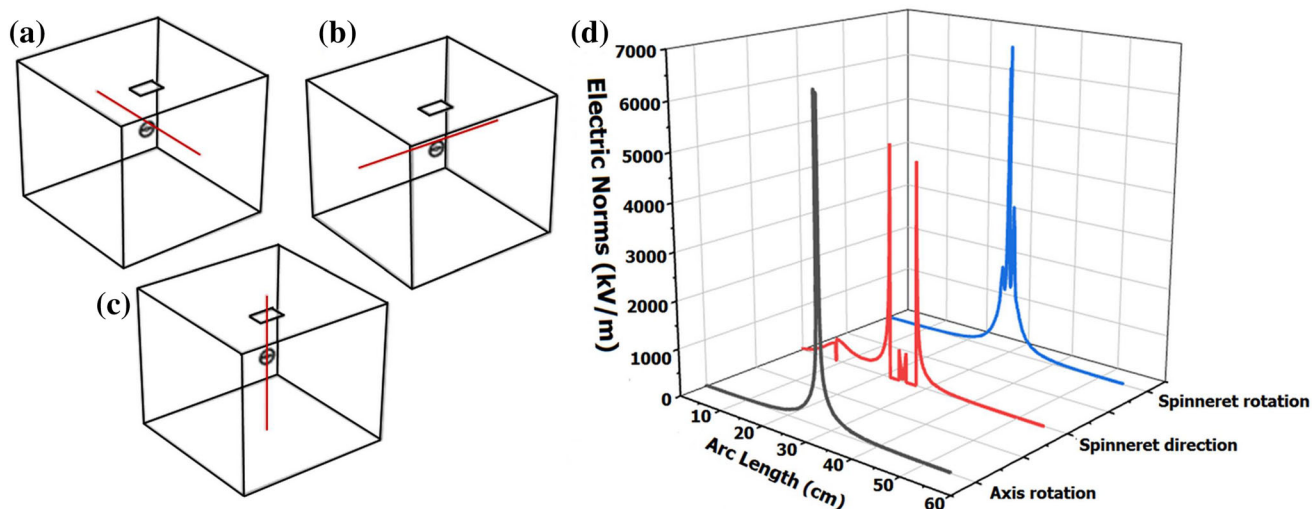
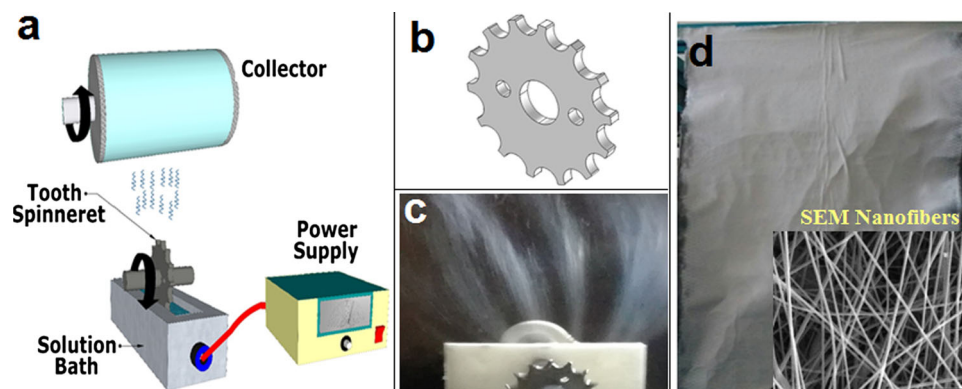


Figure 2 Electric field norm cut line profile **a** in axis direction, **b** in spinning direction, **c** in the spinneret rotation direction, and **d** 3D view of electric norm distribution in axis, spinning and rotation direction.

Fiber morphology and productivity

The effect of PAN concentration on fiber morphology is investigated at different polymer concentrations with a constant applied voltage of 50 kV and collecting distance of 23 cm. Figure 4 shows the SEM images of PAN nanofiber transformation (from beaded to helix shaped micro ribbon) at the different PAN concentrations.

The beaded nanofibers are formed at low concentration of 4 and shift to coarser fiber diameter with increasing concentration to 12. Bead formation at low concentration is due to the low viscosity and surface tension of the solution. The surfaces tension of the solution overcomes the columbic repulsive forces at low viscosity and lead to droplet formation.

The average fiber diameter and production rate are plotted as the function of polymer concentration in Fig. 5a. The maximum diameter difference

147 nm is noted by increasing the concentration from 5 to 7 w/v% with nanofiber diameter 232 ± 40 nm and 379 ± 64 nm, respectively. The higher polymer concentration increases the solution viscosity and results in more chain entanglement due to stronger cohesive forces between PAN chains. This hinders the polymer jet formation and fiber drawing during its flight toward the collector and consequently increases the fiber diameter. The production rate of nanofibers increases from 1.00 to 2.36 g/h by increasing the concentration from 5 to 7 w/v%, respectively. The higher concentration increases the number of polymer jets from the spinneret surface and hence increases the productivity of the electrospinning process. The equation $D = -1333 + 7250 PC$ (where D = diameter; PC = polymer concentration) having high $R^2 = 98.68$ and positive Pearson correlation = 0.993 depicts the

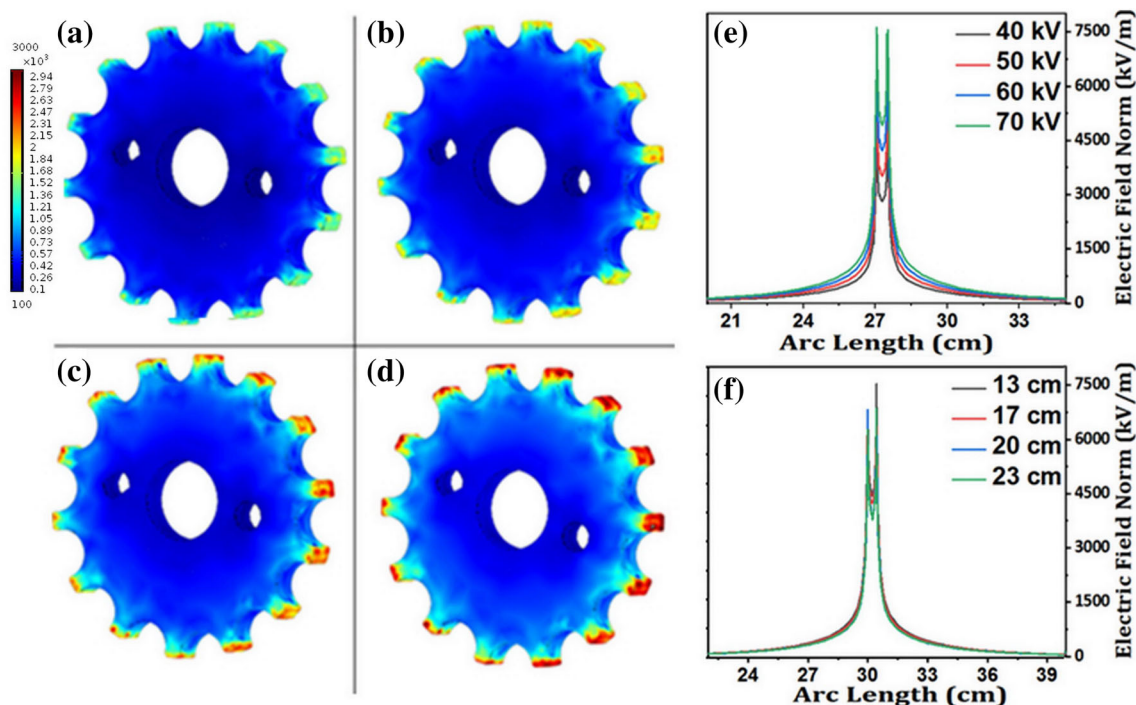


Figure 3 Electric field distribution of toothed wheel spinneret at different voltages **a** 40 kV, **b** 50 kV, **c** 60 kV, **d** 70 kV. Comparison of electric field intensity Norm along axis direction

e at different applied voltages 40–70 kV and 13 cm collecting distance, **f** at different collecting distances 13–23 cm.

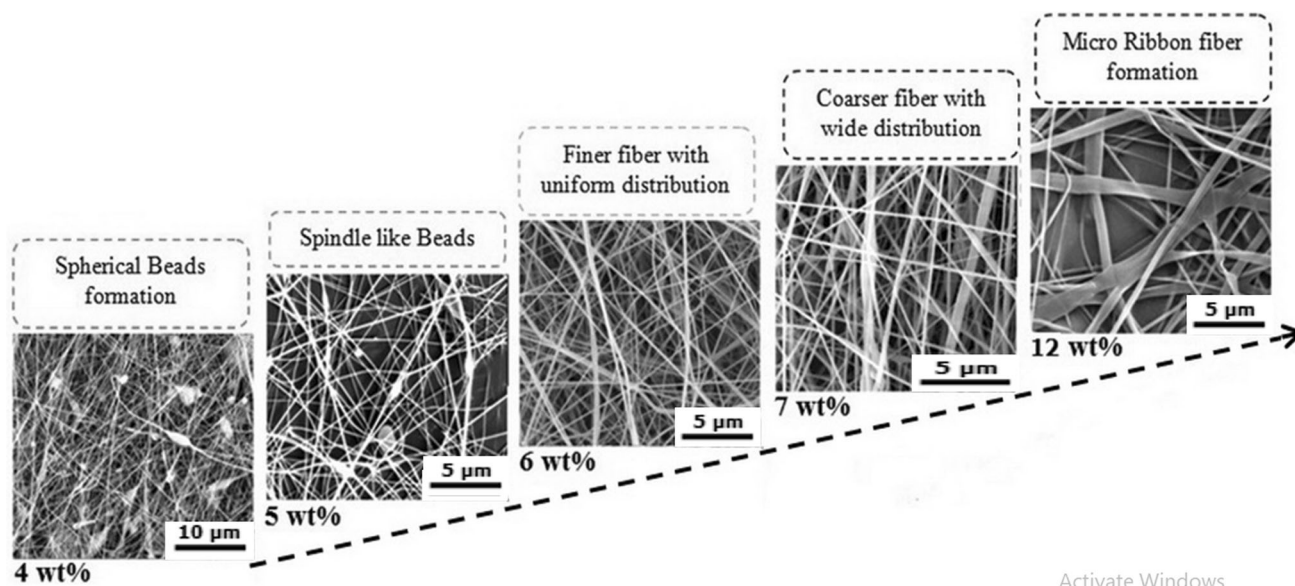


Figure 4 SEM images of PAN nanofiber transformation (from beaded to helix shaped micro ribbon) at different PAN concentrations.

strong positive relation between concentration and fiber diameter.

The impact of applied voltage on fiber morphology is investigated with 6 w/v% PAN/DMF solution at 23 cm collecting distance. Electrospinning process

starts at 30 kV for the toothed wheel spinneret, and random jets form up to 35 kV. Further increase in voltage leads to the smooth nanofiber formation and improves the process stability. The influence of applied voltage on resultant average diameter and

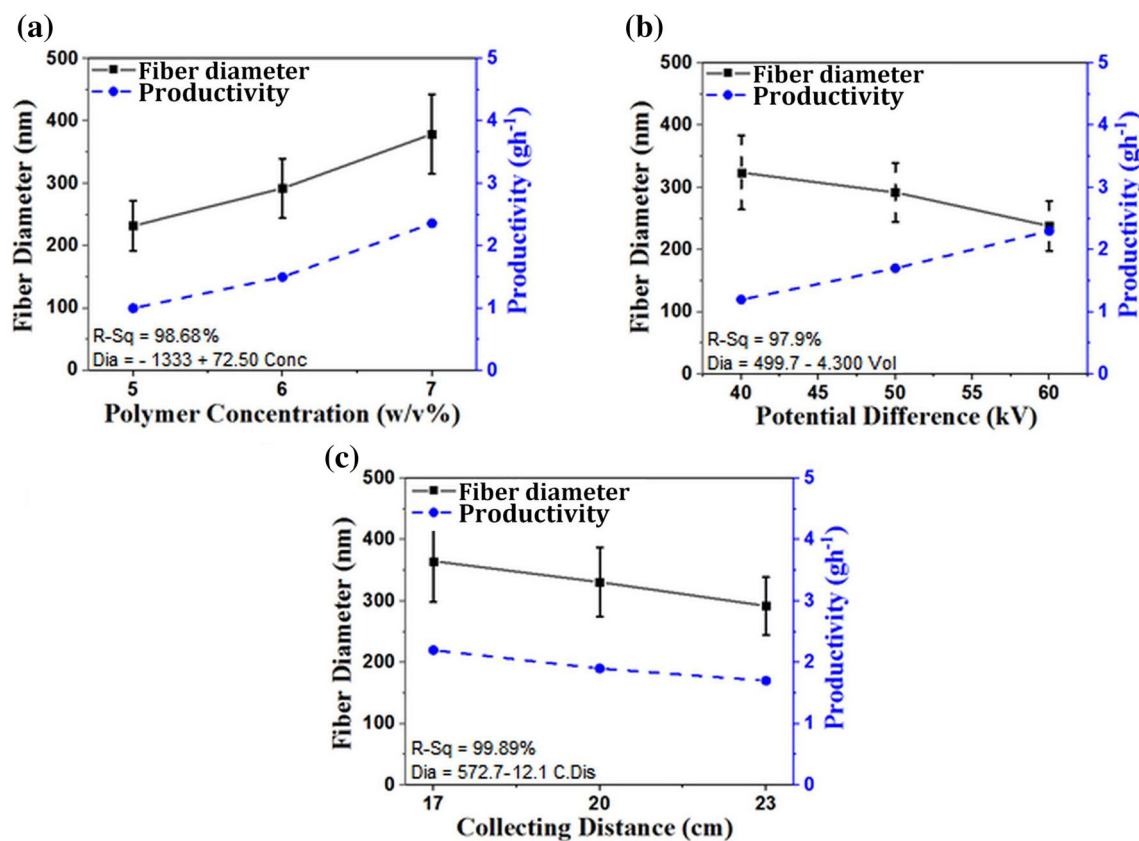


Figure 5 Plot of nanofiber diameter distribution and productivity as a function of **a** polymer concentration 5–7 (applied voltage 50 kV, collecting distance 23 cm), **b** applied voltage 40–60 kV

(polymer concentration 6, collecting distance 23 cm), **c** collecting distance 17–23 cm (polymer concentration 6, applied voltage 50 kV).

productivity is shown in Fig. 5b. The average fiber diameter decreases from 324 ± 59 nm to 238 ± 40 nm by increasing the applied voltage from 40 to 60 kV. The equation $D = 499.7 - 4.3 \text{ PD}$ (where $D = \text{diameter}$; $\text{PD} = \text{potential difference}$) with $R^2 = 97.92$ and Pearson correlation = -0.993 shows the strong inverse relation. The uniform strong electric field is generated at higher voltage, therefore creating stronger electrostatic forces which promote the polymer jet stretching. The higher fiber elongation leads to a decrease in fiber diameter and uniform diameter distribution. Also, the productivity of nanofibers increases from 1.20 to 2.30 g/h by increasing voltage from 40 to 60 kV.

The influence of increasing collecting distance between the spinneret and collector was reported in two ways. The nanofiber diameter reduces at longer collecting distance. This is due to the increase in PAN jets stretching due to the increase in flight time at longer collecting distance. The second effect is that the electrostatic forces decrease at longer collecting

distance, which results in the thicker nanofiber. The effect of collecting distance on fiber diameter and productivity is shown in Fig. 5c. The collecting distance varies from 17 to 23 cm at a constant 6 polymer concentration, and 50 kV applied voltage. This resulted in PAN nanofibers diameter ranging from 365 ± 66 to 292 ± 47 nm.

The equation $D = 572.7 - 12.1 \text{ CD}$ (where $D = \text{diameter}$; $\text{CD} = \text{collecting distance}$) with high $R^2 = 99.8$ and Pearson correlation = -0.999 show the inverse linear relation of collecting distance and diameter. Finer fibers with uniform diameter distribution are produced at a longer distance. However, the decrease in diameter is not much significant as the reduction in electrostatic force and higher fiber elongation balanced the impact on fiber diameter. The productivity of the electrospun nanofiber reduces from 2.20 to 1.70 g/h at collecting distance of 17 and 23 cm, respectively. The production rate decreases due to lower electric field intensity with increase in collecting distance, and hence, fewer polymer jets rise from

spinneret surface. Figure 6 shows the SEM images of nanofiber and histogram of diameter distribution at different polymer concentrations, applied voltages, and collecting distances.

It can be noted that nanofiber diameter distribution is varied at different polymer concentrations and applied voltages. Beadless uniform nanofiber with narrow diameter distribution is obtained at optimized conditioned, which is 6% polymer concentration, 50 kV applied voltage and 23 cm collecting distance.

Regression model of electrospinning parameters and fiber diameter relation

Figure 7 shows the graphs of actual fiber diameter and predicted fiber diameter through the regression equation. The superposition of both plots proves the validation of the regression model. The collective impact of polymer concentration, voltage, and collecting distance on the fiber diameter can be concluded through the regression equation as given below

$$D = 32.11(PC)^2 - 316.8PC - 5.022PD - 9.81CD$$

The high R^2 value of 97.18 and P value less than 0.001 of the regression model is the confirmation of the strong relation of input parameters with the fiber diameter. The high coefficient value of polymer concentration given in above equation depicts the major contribution of 58.17% to influence the fiber diameter. It can be concluded that the effect of polymer concentration is significant than applied voltage and collecting distance. These findings are consistent with the results of previous studies and indicate that polymer solution plays the most important role in determining the fiber diameter [44, 45].

Physical characteristics of electrospun membrane

Electrospun membranes of different thicknesses are obtained for different input variables. Figure 8a–c indicates the influence of polymer concentration, potential difference, and collecting distance on the thickness of nanoweb, respectively.

The thickness of the nanoweb membrane increases from 2.60 to 3.74 mm with increasing concentration from 5 to 7 w/v%. It can be noted that an increase in polymer concentration leads to a higher production

rate, which results in thicker nanoweb. The thickness of the membrane increases from 2.65 to 3.23 mm from 40 to 60 kV applied voltage and 2.83 to 3.06 mm from 17 to 23 cm distance.

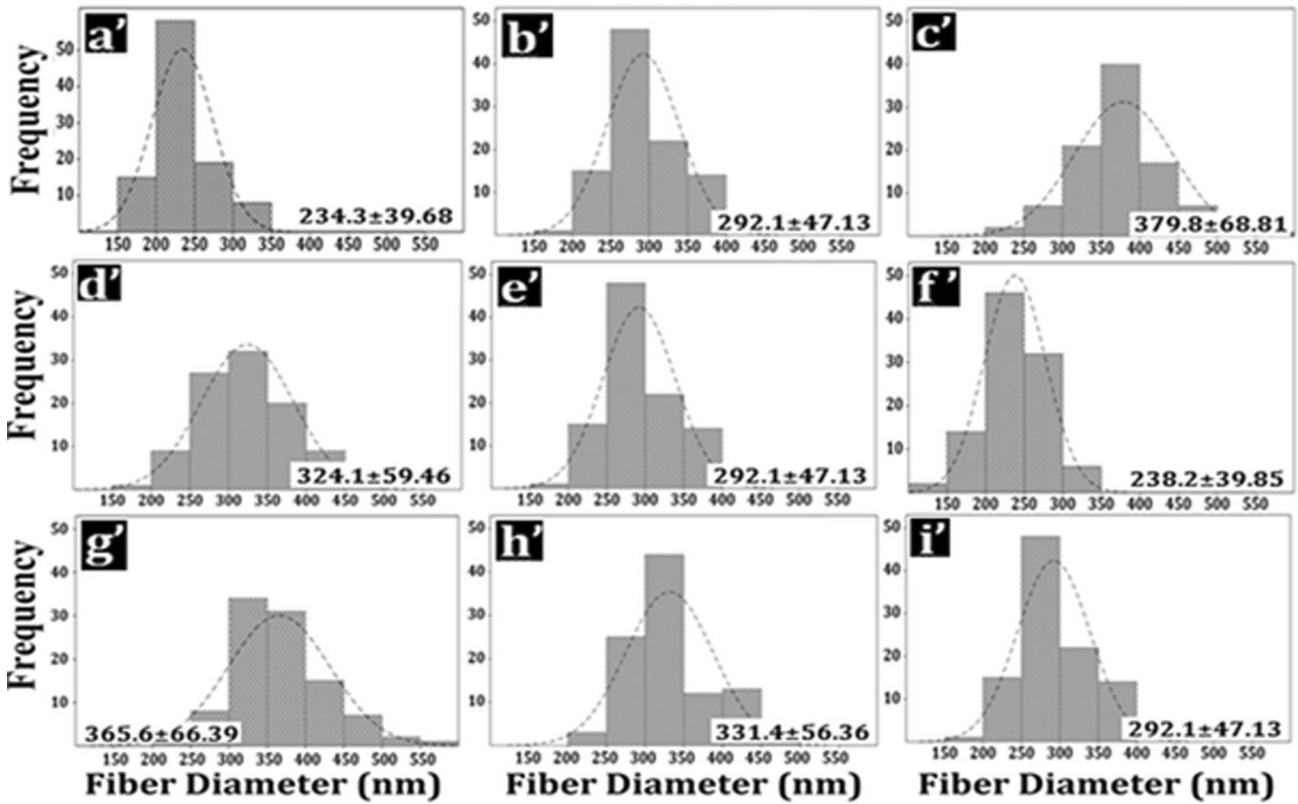
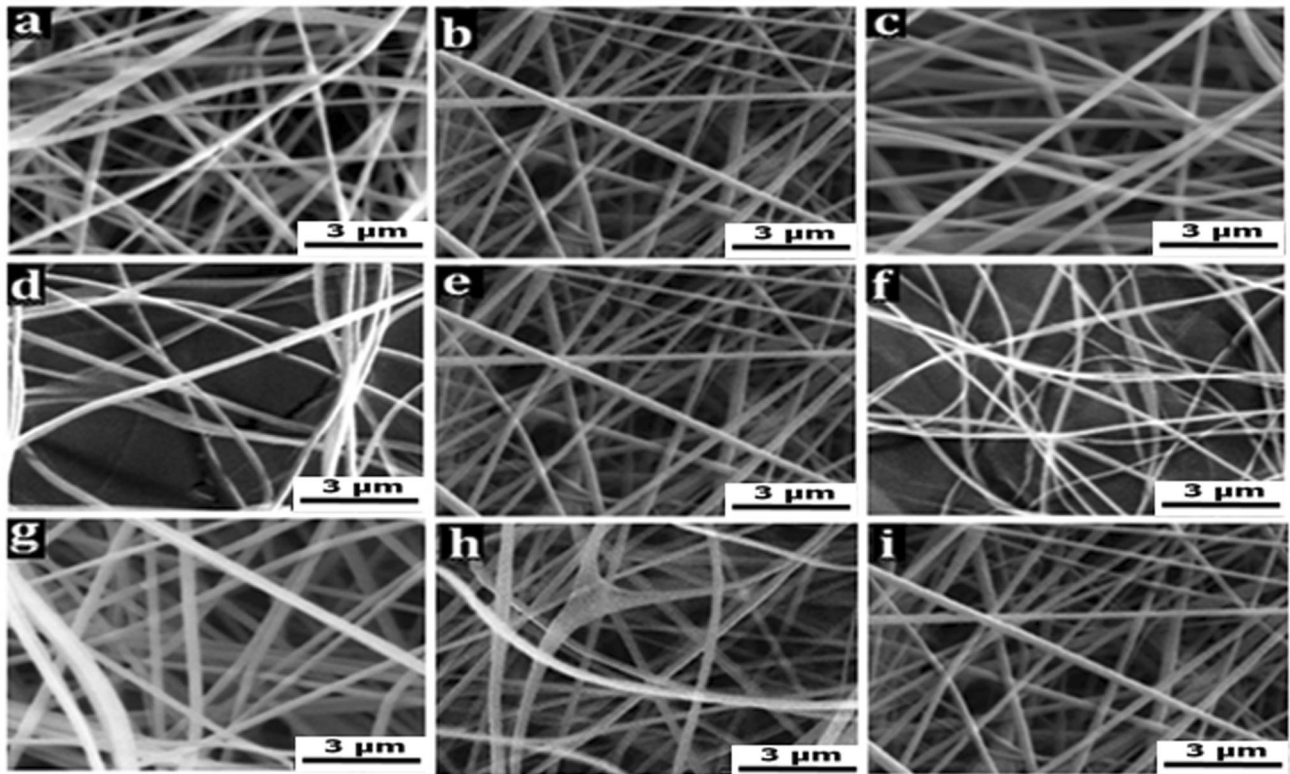
Tensile strength

The tensile strength of PAN nanofiber web is plotted as a function of polymer concentration, applied voltage, and collecting distance, respectively, in Fig. 9a–c. It is noted that tensile strength is improved from 55.33 to 97.41 cN by increasing in PAN concentration from 5 to 6 and from 65.78 to 97.41 cN with an increase in concentration from 6 to 7 at 50 kV applied voltage and 23 cm collecting distance. The increase in tensile strength is attributed to the increase in nanoweb thickness, hence providing more number of nanofibers in cross section. The bead formation and defects are also reduced with increase in polymer concentration. The equation $TS = 53.3 + 21.04 PC$ (where TS = Tensile strength) with $R^2 = 99.36$ and Pearson correlation = 0.964 show a positive co-relation of polymer concentration and tensile strength. The tensile strength is increased from 62.05 to 65.78 cN by increasing 40 to 50 kV applied voltage, and for 50 kV to 60 kV, tensile strength is increased from 65.78 to 70.57 cN. The equation $TS = 44.83 + 0.43 PD$ having $R^2 = 99.49$ and Pearson correlation = 0.997 represent the positive relation of applied voltage and tensile strength. The small coefficient of applied voltage shows little impact on tensile strength. The influence of collecting distance on mechanical properties is noted by varies collecting distance 17 to 23 cm at 6 PAN concentrations and 50 kV applied voltage.

The tensile strength is decreased from 71.26 to 68.89 cN with increase in collecting distance 17 to 20 cm, and for 20 to 23 cm, tensile strength is reduced from 68.89 to 65.68 cN. The equation $TS = 86.91 - 0.913 CD$ having $R^2 = 99.36$ and Pearson correlation = -0.997 indicates the inverse relation of collecting distance and tensile strength. However, the impact of collecting distance is not much significant.

Regression model of electrospinning parameters and tensile strength relation

The relation of tensile strength and electrospinning parameters can be given by equation as given below



◀ **Figure 6** SEM image of nanofibers under the influence of polymer concentration 5–7 at applied voltage 50 kV and collecting distance 23 cm (a–c), applied voltage 40–60 kV at polymer concentration 6 and collecting distance 23 cm (d–f), collecting distance 17–23 cm at polymer concentration 6, applied voltage 50 kV (g–i) an histogram of diameter distribution polymer concentration 5–7 (a'–c'), applied voltage 40–60 kV (d'–f'), collecting distance 17–23 cm (g'–i').

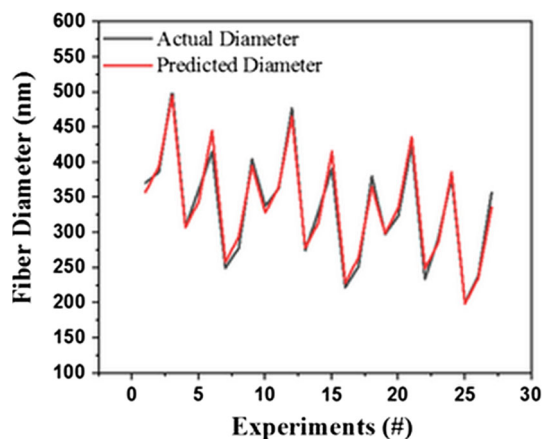
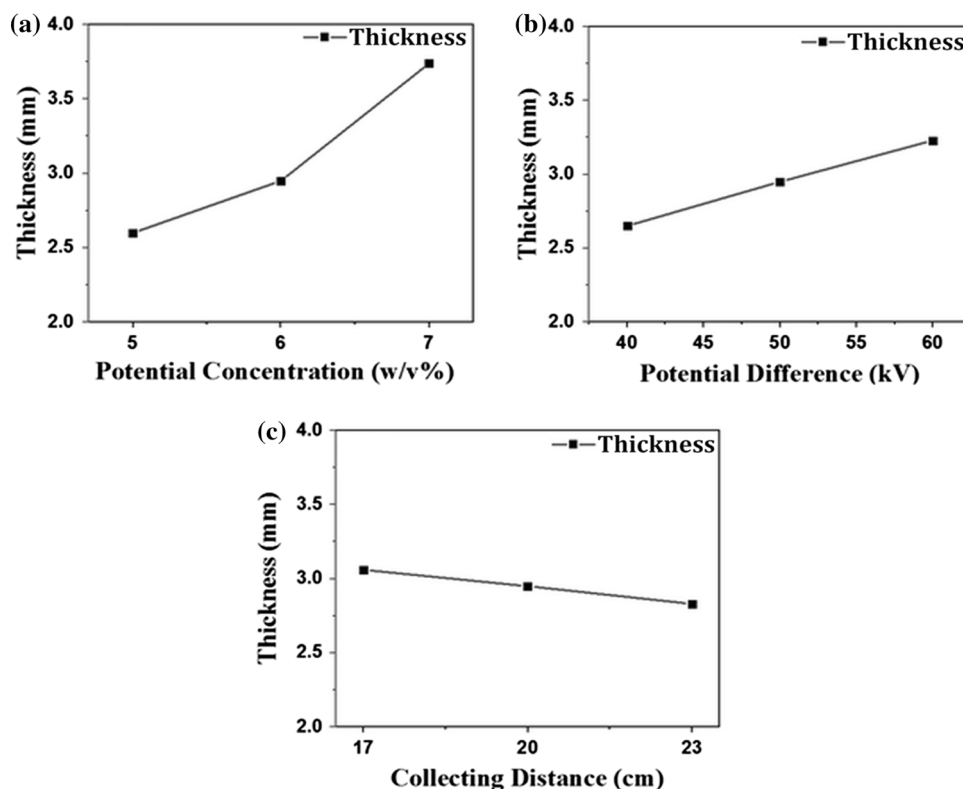


Figure 7 The plot of actual versus predicted nanofiber fiber diameters.

Figure 8 Comparison of nanoweb thickness as a function of **a** polymer concentration, **b** potential difference, **c** collecting distance.



$$TS(\text{cN}) = 21.04PC + 0.42PD - 0.317CD - 71.4$$

The high R^2 value of 85.63 indicates the validation of the linear relation. The coefficient of polymer concentration in the regression model is high compared to the coefficient of applied voltage and collecting distance. This depicts that the influence of polymer concentration is much significant than the applied voltage and collecting distance. Figure 10 shows the comparison of actual and predicted tensile strength.

Air permeability

The influence of electrospinning parameters polymer concentration, applied voltage, and spinning distance on the air permeability of nanoweb is shown in Fig. 11. The air permeability of nanomembrane depends highly on the thickness of nanoweb and fiber distribution. In Fig. 11a air permeability shows the irregular trend at different levels of polymer concentration. The air permeability value is 25.30 mm/s at 5 polymer concentration. It is noted that at low concentration, a thin nanoweb containing a smaller number of nanofibers in cross section is developed due to less produc-

Figure 9 Comparison of tensile strength as a function of a polymer concentration, b applied potential, c collecting distance.

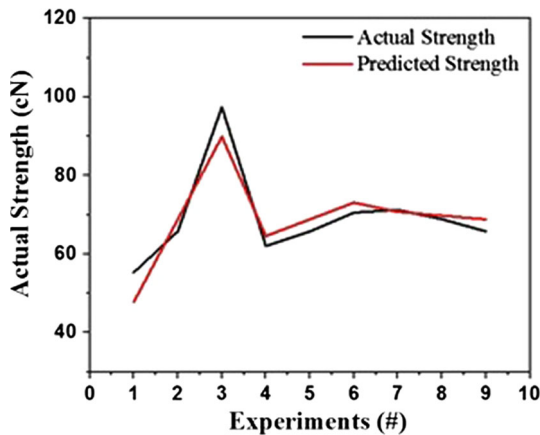
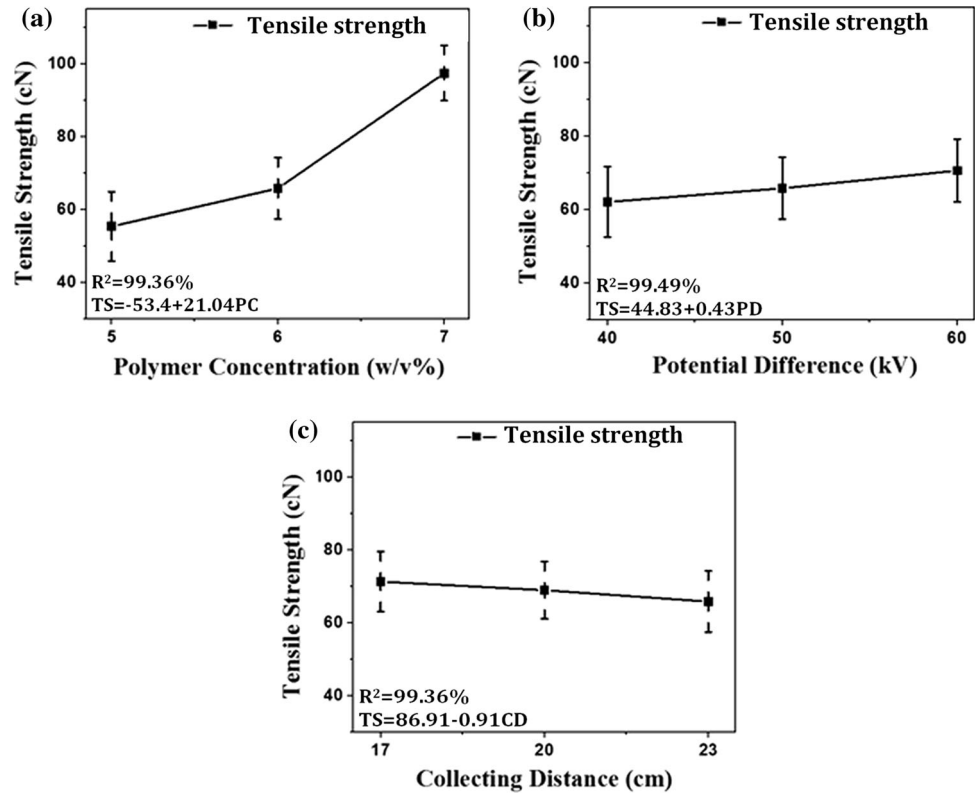


Figure 10 Comparison of actual versus predicted nanoweb tensile strength.

tion rate. Moreover, the formation of the bead at low concentration creates voids between the nanofibers. Hence, both parameters reduce air resistance and provide an easy path to air flow. Similarly, the air permeability is noted at 32.76 mm/s at 7 polymer concentration. At high concentration, coarser fibers are produced and create wide spaces between the fibers. This improves the air current through nanoweb. Although the thicker membrane is obtained by increasing the polymer concentration, the impact of

voids is prominent. Abuzade et al. also studied the air permeability of electrospun nanoweb and concluded that higher polymer concentration at constant value of applied voltage and spinning distance can result in higher porosity and thereby higher air permeability per unit weight of nanoweb [46]. Contrarily, the air permeability value is lowered 17.95 mm/s at 6 concentration compared to 5 and 7. Fine nanofibers of uniform diameter distribution are formed at 6, which minimize the free spaces between the nanofibers and reduce the air flow through nanoweb. The equation $AP = 3.0 + 3.73 PC$ (where $AP =$ air permeability) having R^2 value of 25.37 and Pearson correlation of 0.504 cannot predict the relation of air permeability and polymer concentration.

The air permeability and applied voltage have a linear inverse relation. The air permeability reduces from 21.33 to 14.97 mm/s by increasing the applied voltage from 40 to 60 kV. High production rate and finer nanofibers with uniform diameter distribution at high applied voltage make the nanoweb less permeable. The equation $AP = 34.006 + 31.83 PD$ with 99.89 R^2 value and -0.999 Pearson correlation show the inverse linear relation of air permeability and applied voltage.

Figure 11 Comparison of air permeability as a function of **a** polymer concentration, **b** applied potential, **c** collecting distance.

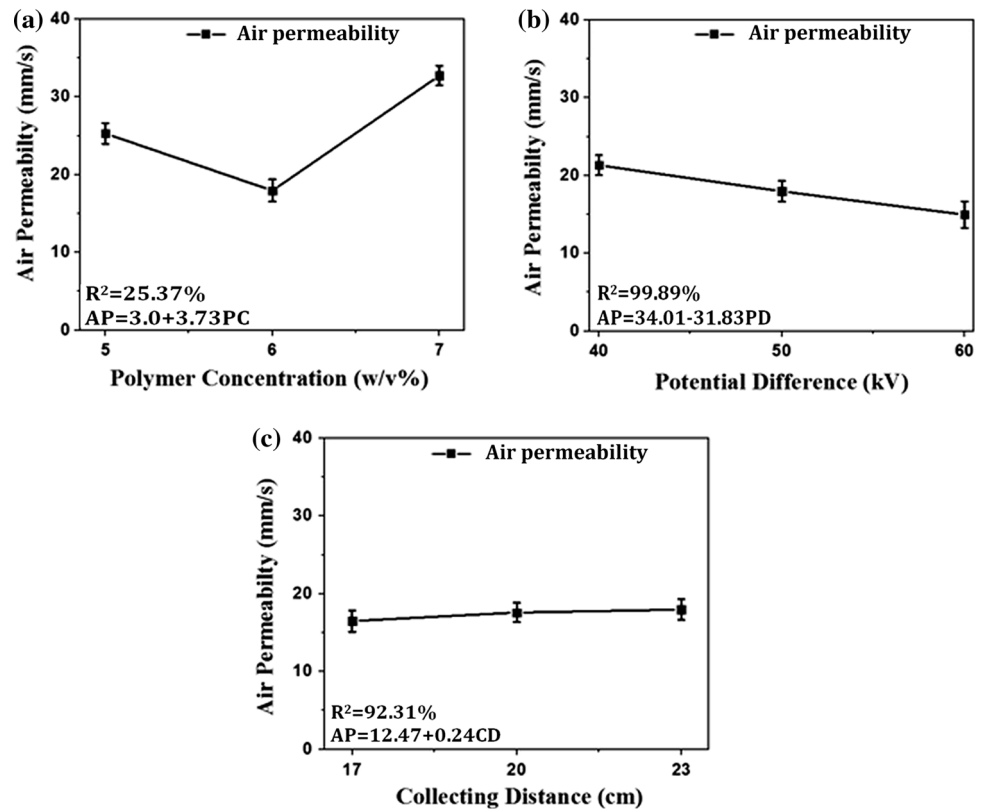


Figure 11c shows an increase of 1.47 mm/s air current by increasing collecting distance from 17 to 23 cm. The equation $AP = 12.47 + 0.2444 CD$ having 92.31 R^2 value and 0.961 Pearson correlation show the relation of air permeability and collecting distance. The small coefficient of collecting distance indicates that effect of collecting distance on the air permeability of PAN nanoweb is not much significant.

Regression model air permeability and electrospinning parameters

The relation of electrospinning parameter and air permeability can be derived as

$$AP(\text{mm/s}) = 3.73PC - 0.318PD + 0.848CD - 4.9$$

The R^2 value of the regression model is very low at 29.85. Moreover, the coefficient value of the input variable is very small. This indicates that the regression model has little significance and cannot explain the true relation of input and output variables. Figure 12 shows the comparison of actual and predicted values of air permeability. The lack of fitting of both lines also proves the unreliability of the regression model. This is due to that beaded nanofibers are

obtained at low concentration, and coarser fibers are formed at high concentration. Beaded and coarser nanofiber both increase the air permeability through the nanoweb as discussed above. However, both are not in proportion simultaneously at different polymer concentrations, hence reducing the fitting of both curves lines in the graph.

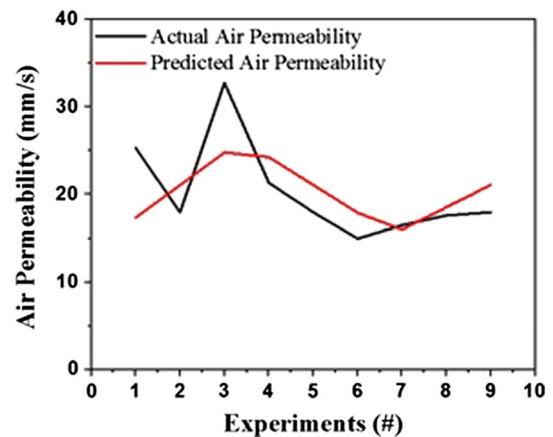


Figure 12 Plot of actual versus predicted nanoweb air permeability.

Conclusion

In this study, a novel toothed wheel spinneret was developed to improve the needleless electrospinning process with uniform and concentrated electric field norm at the spinneret surface. The uniform electric field improved the nanofibers production rate, uniform diameter distribution in nanoweb, and reduced the threshold voltage. The finite element method was used to evaluate the electric field norm around toothed wheel spinneret. The simulation results predicted that strong uniform electric field intensity was developed at the surface of the toothed wheel spinneret, which lowered the threshold voltage to initiate the electrospinning process. The impact of the polymer concentration and process variables on the fiber morphology and productivity was evaluated. It was found that the influence of polymer concentration was significant than potential difference and collecting distance. The physical properties, such as tensile strength and air permeability of the nanofibrous membranes, were also investigated. The tensile properties of the nanomembrane enhanced with the increase in membrane thickness at high concentration and applied voltage. Air permeability trend for the concentration was not linear, and the lowest air permeability was observed at 6% due to fine nanofiber and uniform diameter distribution. This effectively designed novel toothed wheel spinneret has the potential to improve the electrospinning process with the development of uniform nanofibrous membrane and high productivity.

Acknowledgements

This research work was partially sponsored by Higher Education Commission, Pakistan with Grant No. 20-4179/NRPU/R&D/HEC/14.

Authors' contribution

This work was partially carried out at the Bahauddin Zakariya University College of Textile Engineering (BZU), Multan and National Textile University, Faisalabad. MBQ conceived the idea and supervised the project. AA and AK planned and performed the experiments, collected and analyzed the data. AA and BM designed the spinneret geometry and

analyzed the electric field Norm at Comsol. AS analyzed the structural design of spinneret and reviewed the results obtained from Comsol. AH, SA, SA and RT assisted with the experiments and characterizations. AN and UA analyzed the structure properties of nanofiber and derived the relations among relevant parameters. MBQ, ZK co-wrote the manuscript. All the authors discussed the results and commented on the manuscript.

Compliance with ethical standards

Conflict of interest The authors declare that they have no conflict of interest.

References

- [1] Sun KC, Arbab AA, Sahito IA et al (2017) A PVdF-based electrolyte membrane for a carbon counter electrode in dye-sensitized solar cells. *RSC Adv* 7:20908–20918. <https://doi.org/10.1039/C7RA00005G>
- [2] Qadir MB, Sahito IA, Arbab AA et al (2018) Synthesis of vastly porous and highly functional titanium nanotubes and their application in Dye-sensitized Solar Cells. In: The 16th international nanotech symposium and nano-convergence expo. Korea Nano Technology Research Society, Korea, South Korea, p 896
- [3] Memon AA, Arbab AA, Sahito IA et al (2017) Facile fabrication of activated charcoal decorated functionalized multi-walled carbon nanotube electro-catalyst for high performance quasi-solid state dye-sensitized solar cells. *Electrochim Acta* 234:53–62. <https://doi.org/10.1016/j.electacta.2017.03.018>
- [4] Jabbar A, Afzal A, Malik ZA et al (2017) Mechanical behavior of nanocellulose coated jute/green epoxy composites. In: 1st international conference on technical textiles (ICTT-2017). National Textile University, National Textile University, Faisalabad, Pakistan, pp 80–82
- [5] Sahito IA, Sun KC, Arbab AA et al (2016) Flexible and conductive cotton fabric counter electrode coated with graphene nanosheets for high efficiency dye sensitized solar cell. *J Power Sources* 319:90–98. <https://doi.org/10.1016/j.jpowsour.2016.04.025>
- [6] Sahito IA, Sun KC, Arbab AA et al (2015) Integrating high electrical conductivity and photocatalytic activity in cotton fabric by cationizing for enriched coating of negatively charged graphene oxide. *Carbohydr Polym* 130:299–306. <https://doi.org/10.1016/j.carbpol.2015.05.010>
- [7] Sahito IA, Sun KC, Arbab AA et al (2015) Graphene coated cotton fabric as textile structured counter electrode for

- DSSC. *Electrochim Acta* 173:164–171. <https://doi.org/10.1016/j.electacta.2015.05.035>
- [8] Qadir MB, Sun KC, Sahito IA et al (2015) Composite multi-functional over layer: a novel design to improve the photo-voltaic performance of DSSC. *Sol Energy Mater Sol Cells* 140:141–149. <https://doi.org/10.1016/j.solmat.2015.04.011>
- [9] Arbab AA, Sun KC, Sahito IA et al (2015) Multiwalled carbon nanotube coated polyester fabric as textile based flexible counter electrode for dye sensitized solar cell. *Phys Chem Chem Phys* 17:12957–12969. <https://doi.org/10.1039/C5CP00818B>
- [10] Sun KC, Qadir MB, Jeong SH (2014) Hydrothermal synthesis of TiO₂ nanotubes and their application as an over-layer for dye-sensitized solar cells. *RSC Adv* 4:23223–23230. <https://doi.org/10.1039/C4RA03266G>
- [11] Qadir MB, Li Y, Sahito IA et al (2016) Highly functional TNTs with superb photocatalytic, optical, and electronic performance achieving record PV efficiency of 10.1% for 1D-based DSSCs. *Small* 12:4508–4520. <https://doi.org/10.1002/smll.201601058>
- [12] Arbab AA, Sun KC, Sahito IA et al (2015) Fabrication of highly electro catalytic active layer of multi walled carbon nanotube/enzyme for Pt-free dye sensitized solar cells. *Appl Surf Sci* 349:174–183. <https://doi.org/10.1016/J.APSUSC.2015.04.199>
- [13] Mengal N, Sahito IA, Arbab AA et al (2016) Fabrication of a flexible and conductive lyocell fabric decorated with graphene nanosheets as a stable electrode material. *Carbohydr Polym* 152:19–25. <https://doi.org/10.1016/J.CARBPOL.2016.06.099>
- [14] Arbab AA, Sun KC, Sahito IA et al (2016) A novel activated-charcoal-doped multiwalled carbon nanotube hybrid for quasi-solid-state dye-sensitized solar cell outperforming Pt electrode. *ACS Appl Mater Interfaces* 8:7471–7482. <https://doi.org/10.1021/acsami.5b09319>
- [15] He J-H, Wan Y-Q, Yu J-Y (2008) Effect of concentration on electrospun polyacrylonitrile (PAN) nanofibers. *Fibers Polym* 9:140–142. <https://doi.org/10.1007/s12221-008-0023-3>
- [16] Park BK, Um IC (2018) Effect of molecular weight on electro-spinning performance of regenerated silk. *Int J Biol Macromol* 106:1166–1172. <https://doi.org/10.1016/j.ijb.2018.06.099>
- [17] Zhao YY, Yang QB, Lu XF et al (2005) Study on correlation of morphology of electrospun products of polyacrylamide with ultrahigh molecular weight. *J Polym Sci Part B Polym Phys* 43:2190–2195. <https://doi.org/10.1002/polb.20506>
- [18] Liu Y, Dong L, Fan J et al (2011) Effect of applied voltage on diameter and morphology of ultrafine fibers in bubble electrospinning. *J Appl Polym Sci* 120:592–598. <https://doi.org/10.1002/app.33203>
- [19] Jiang G, Zhang S, Qin X (2016) Effect of processing parameters on free surface electrospinning from a stepped pyramid stage. *J Ind Text* 45:483–494. <https://doi.org/10.1177/1528083714537101>
- [20] Hekmati AH, Rashidi A, Ghazisaeidi R, Drean J-Y (2013) Effect of needle length, electrospinning distance, and solution concentration on morphological properties of polyamide-6 electrospun nanowebs. *Text Res J* 83:1452–1466. <https://doi.org/10.1177/0040517512471746>
- [21] Chatterjee A, Deopura BL (2006) Thermal stability of polypropylene/carbon nanofiber composite. *J Appl Polym Sci* 100:3574–3578. <https://doi.org/10.1002/app.22864>
- [22] Liu Y, Zhou S, Gao Y, Zhai Y (2019) Electrospun nanofibers as a wound dressing for treating diabetic foot ulcer. *Asian J Pharm Sci* 14:130–143. <https://doi.org/10.1016/J.AJPS.2018.04.004>
- [23] Levitt AS, Alhabeab M, Hatter CB et al (2019) Electrospun MXene/carbon nanofibers as supercapacitor electrodes. *J Mater Chem A* 7:269–277. <https://doi.org/10.1039/C8TA09810G>
- [24] Arbab AA, Sun KC, Sahito IA et al (2016) A novel activated-charcoal-doped multiwalled carbon nanotube hybrid for quasi-solid-state dye-sensitized solar cell outperforming Pt electrode. *ACS Appl Mater Interfaces* 8:7471–7482. <https://doi.org/10.1021/acsami.5b09319>
- [25] El Fawal GF, Hassan HS, El-Aassar MR, Elkady MF (2019) Electrospun polyvinyl alcohol nanofibers containing titanium dioxide for gas sensor applications. *Arab J Sci Eng* 44:251–257. <https://doi.org/10.1007/s13369-018-3529-z>
- [26] Zhang L, Aboagye A, Kelkar A et al (2014) A review: carbon nanofibers from electrospun polyacrylonitrile and their applications. *J Mater Sci* 49:463–480. <https://doi.org/10.1007/s10853-013-7705-y>
- [27] Nazir A, Khaliq Z, Ali Z et al (2018) Development of electrospun nanofiber incorporated facemask and study of its performance and comfort properties. In: International conference on innovation and entrepreneurship in textiles (IE-TEX-2018). National Textile University, Faisalabad, Pakistan, p 4
- [28] Khaliq Z, Qadir MB, Shahzad A et al (2018) Development of electrospun porous carbon fibers from cellulose/polyacrylonitrile blend. In: 20th International conference on polymer products and engineering. World Academy of Science, Engineering and Technology, Cape Town, South Africa, p 2364
- [29] Nazir A, Qadir MB, Malik ZA et al (2017) Filtration and comfort properties of face masks containing polyamide electro-spun nanowebs. In: 1st International conference on

- technical textiles (ICTT-2017). National Textile University, Faisalabad, Pakistan, p 66
- [30] Park I, Kim SS, Kim W (2018) Multi-jet electrospinning with high-throughput using a coaxial grooved nozzle and two fluids. *Polym Eng Sci* 58:416–421. <https://doi.org/10.1002/pen.24588>
- [31] Kumar A, Wei M, Barry C et al (2010) Controlling fiber repulsion in multijet electrospinning for higher throughput. *Macromol Mater Eng* 295:701–708. <https://doi.org/10.1002/mame.200900425>
- [32] Fang S-P, Jao P, Senior DE et al (2017) Study on high throughput nanomanufacturing of photopatternable nanofibers using tube nozzle electrospinning with multi-tubes and multi-nozzles. *Micro Nano Syst Lett* 5:1–10. <https://doi.org/10.1186/s40486-017-0044-z>
- [33] Dosunmu OO, Chase GG, Kataphinan W, Reneker DH (2006) Electrospinning of polymer nanofibres from multiple jets on a porous tubular surface. *Nanotechnology* 17:1123–1127. <https://doi.org/10.1088/0957-4484/17/4/046>
- [34] Lin T (2012) Needleless electrospinning: a practical way to mass production of nanofibers. *J Text Sci Eng* 02:1–3. <https://doi.org/10.4172/2165-8064.1000e109>
- [35] Yarin AL, Zussman E (2004) Upward needleless electrospinning of multiple nanofibers. *Polymer (Guildf)* 45:2977–2980. <https://doi.org/10.1016/j.polymer.2004.02.066>
- [36] Liu Y, He J-H (2007) Bubble electrospinning for mass production of nanofibers. *Int J Nonlinear Sci Numer Simul* 8:393–396. <https://doi.org/10.1515/IJNSNS.2007.8.3.393>
- [37] Thoppey NM, Bochinski JR, Clarke LI, Gorga RE (2010) Unconfined fluid electrospun into high quality nanofibers from a plate edge. *Polymer (Guildf)* 51:4928–4936. <https://doi.org/10.1016/J.POLYMER.2010.07.046>
- [38] Chaloupek J, Jirsak O, Kotek V, Lukas D, Lenka Martinova FS (2004) A method of nanofibres production from a polymer solution using electrostatic spinning and a device for carrying out the method. WO 2005/024101 A1
- [39] Thoppey NM, Bochinski JR, Clarke LI, Gorga RE (2011) Edge electrospinning for high throughput production of quality nanofibers. *Nanotechnology* 22:1–11. <https://doi.org/10.1088/0957-4484/22/34/345301>
- [40] Ali U, Niu H, Aslam S et al (2017) Needleless electrospinning using sprocket wheel disk spinneret. *J Mater Sci* 52:7567–7577. <https://doi.org/10.1007/s10853-017-0989-6>
- [41] Wei L, Yu H, Jia L, Qin X (2018) High-throughput nanofiber produced by needleless electrospinning using a metal dish as the spinneret. *Text Res J* 88:80–88. <https://doi.org/10.1177/0040517516677232>
- [42] Liu Z, Ang KKJ, He J (2017) Needle-disk electrospinning inspired by natural point discharge. *J Mater Sci* 52:1823–1830. <https://doi.org/10.1007/s10853-016-0472-9>
- [43] Hassan MA, Ali U, Shahzad A et al (2018) Bullet-spinneret based needleless electrospinning; a versatile way to fabricate continuous nanowebs at low voltage. *Mater Res Express* 6:025053. <https://doi.org/10.1088/2053-1591/aaf137>
- [44] Amiraliyan N, Nouri M, Kish MH (2009) Electrospinning of silk nanofibers. I. An investigation of nanofiber morphology and process optimization using response surface methodology. *Fibers Polym* 10:167–176. <https://doi.org/10.1007/s12221-009-0167-9>
- [45] Dehghan SF, Golbabaee F, Maddah B et al (2016) Optimization of electrospinning parameters for polyacrylonitrile-MgO nanofibers applied in air filtration. *J Air Waste Manag Assoc* 66:912–921. <https://doi.org/10.1080/10962247.2016.1162228>
- [46] Abuzade RA, Zadhoush A, Gharehaghaji AA (2012) Air permeability of electrospun polyacrylonitrile nanoweb. *J Appl Polym Sci* 126:232–243. <https://doi.org/10.1002/app.36774>

Publisher's Note Springer Nature remains neutral with regard to jurisdictional claims in published maps and institutional affiliations.